Proceedings of the International Symposium on Physics of Materials (ISPMA13)

# Mechanisms of Plastic Deformation in Ti–Nb–Zr–Ta Based Biomedical Alloys with Fe and Si Content

J. Stráský*, P. Harcuba, K. Horváth, M. Janeček
Charles University in Prague, Department of Physics of Materials, Ke Karlovu 5, 121 16, Praha 2, Czech Republic

Specialized beta titanium alloys containing biocompatible elements (Nb, Zr, Ta) are increasingly considered as a material for orthopaedic implants. In this study, small additions of Fe and Si are used to increase the strength of commercial Ti–35Nb–7Zr–5Ta (TNZT) alloy. Six different advanced alloys with iron content up to 2 wt% and silicon content up to 1 wt% were manufactured by arc melting and hot forging. Flow curves were determined from tensile tests carried out at room temperature. The yield stress is increased from 450 MPa to 700 MPa due to small Fe and Si additions. Fe causes solid solution strengthening exhibited by sharp yield point and significant work hardening. $(Ti,Zr)_5Si_3$ intermetallic particles further increase the strength via precipitation hardening. An unusual serrated yielding behaviour of benchmark TNZT alloy is caused by twinning as shown by acoustic emission measurement and electron backscattered diffraction analysis.

DOI: 10.12693/APhysPolA.128.574
PACS: 81.05.Bx, 81.40.Cd, 81.70.Bt, 81.40.Lm

## 1. Introduction

Titanium alloys are extensively applied in orthopaedic implants due to their superior mechanical properties, excellent corrosion resistance, and favourable biocompatibility. There are numerous studies reviewing the outstanding properties of these materials for medical use [1–4]. Excellent biocompatibility of titanium was proven by many authors both *in vitro* and *in vivo* [5, 6]. However, less often reported mechanical properties are of major interest in this work. The biggest current interest is focused on metastable $\beta$-titanium alloys with increased biocompatibility and decreased elastic modulus to avoid stress-shielding and increase of life-time of an implant [7]. Ti–Nb–Zr–Ta alloys are the mostly investigated alloy system. Different types of Ti–Nb–Ta–Zr (sometimes abbreviated as TNTZ or TNZT) have been developed. The two mostly used and investigated compositions are Ti–29Nb–13Ta–4.6Zr [8] and Ti–35Nb–7Zr–5Ta. The latter alloy was developed in 1990s in USA and patented in 1999 [9]. This TNZT composition was used as a benchmark material for experimental investigations in the present work. The considerable disadvantage of this alloy is its relatively low strength. Despite both Zr and Ta provide some solution strengthening compared to Ti–Nb binary alloys [10, 11], the ultimate tensile strength reaches only around 500 MPa that is significantly lower than the ultimate tensile strength (UTS) of the most common Ti–6Al–4V alloy (≈800 MPa) The strengthening effect of iron and silicon is investigated in this work. Fe causes simple solution strengthening in $\beta$-alloys [12], whereas Si contributes to hardening via the creation of dispersed precipitates $(Ti,Zr)_5Si_3$ [13, 14]. Si contents of 0.2–0.4 wt% is often utilized in high-strength and high-temperature alloys in aerospace industry in order to increase the strength and to suppress excessive creep [15, 16].

## 2. Material and experimental procedure

A TNZT alloy with chemical composition Ti–35.3Nb–7.3Zr–5.7Ta (wt%) was used as a benchmark. Six different tailored alloys utilizing 0–2 wt% Fe and 0–1 wt% Si in excess of Ti content were manufactured and their chemical compositions are summarized in the Table.

TABLE

Chemical composition of alloys based on the Ti–35.3Nb–5.7Ta–7.3Zr alloy (TNZT), Si and Fe contents are given in wt%.

| | |
|---|---|
| TNZT | TNZT+0.5Si+1Fe |
| TNZT+1Si | TNZT+0.5Si+2Fe |
| TNZT+2Fe | TNZT+1Si+1Fe |

All alloys were prepared by arc melting of pure elements under a low pressure of clean He (350 mbar) Each part of the sample was remelted at least six times by electric arc to ensure homogeneity. Samples of approximate weight 200 g were subsequently homogenized at 1400 °C for two hours and furnace cooled. The oxygen content is below 0.04 wt% and the nitrogen content below 200 ppm after homogenization. The material was then forged using a forging hammer into shape of rods that were finally machined to the diameter of 14 mm. Material was heated to approximately 1100 °C before and during forging, however, the forging temperature was not precisely controlled.

Tensile tests were conducted at room temperature with a $10^{-4}$ $s^{-1}$ strain rate, using an Instron 5882 computer controlled machine. Scanning electron microscope FEI Quanta 200F (FEG) operating at the accelerating voltage of 20 kV was used. Electron backscattered diffraction (EBSD) was analyzed using DigiView3 EBSD camera

*corresponding author; e-mail: josef.strasky@gmail.com

from company EDAX and OIM (orientation imaging mapping) software was employed for EBSD observations. A computer-controlled DAKEL-CONTI-4 acoustic emission system was used to monitor acoustic emission (AE) during the tensile test. Four channels with different amplification (0–20–30–40 dB) and 2 MHz sampling frequency were used to detect and store data. More details on the method and the data analysis are reported in [17, 18].

## 3. Results and discussion

Figure 1 shows the yield stress and the UTS of prepared alloys in the as-forged condition. Presented values are mean values from three samples and the standard deviation is shown by the error bar. The yield stress of the benchmark TNZT alloy is below 500 MPa. Fe causes solid solution strengthening due to different electron bonding and Si causes precipitation strengthening. The combined effect of Fe and Si leads to even increased strength. The TNZT–2Fe–0.5Si alloy yields above 700 MPa and its ultimate strength is higher than 800 MPa. Such values are relatively high, considering that the metastable beta alloys were not aged to achieve hardening by $\alpha$-phase precipitates.

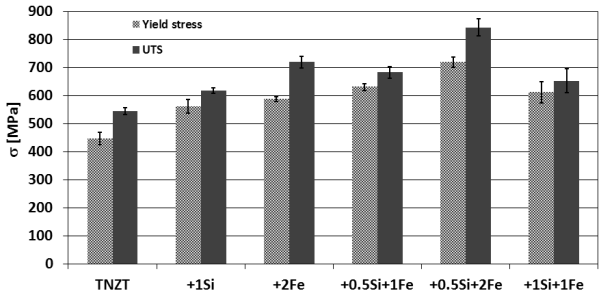


Fig. 1. Yield stress and (UTS).

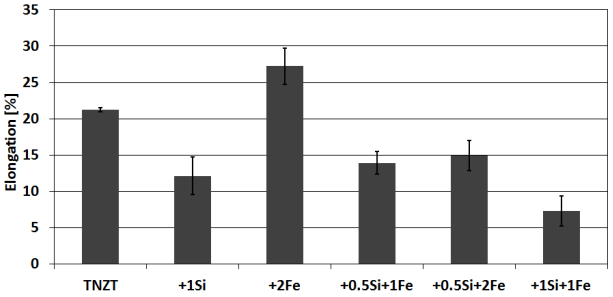


Fig. 2. Total elongation (A5 elongation — length of active part of the specimens equals 5× diameter).

Figure 2 summarizes the total plastic elongation. All alloys are ductile at room temperature, but Si significantly reduces the total elongation. Fe content increased total elongation when compared to the benchmark alloy. This effect is associated with work hardening and is discussed below based on analysis of flow curves.

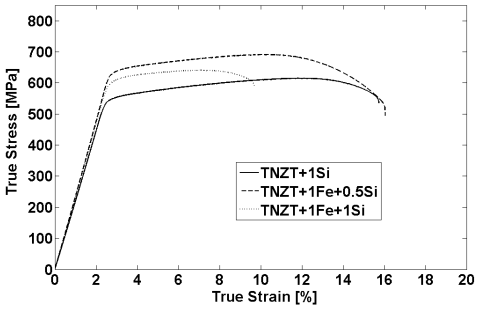


Fig. 3. Flow curves — alloys containing less than 2 wt% Fe, common plastic deformation behaviour is observed.

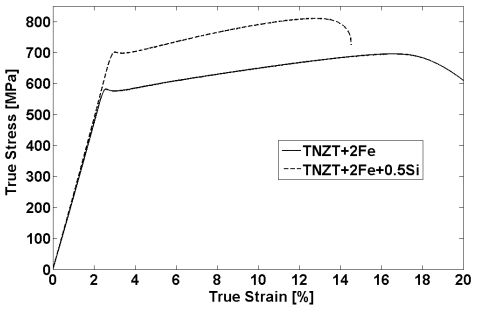


Fig. 4. Flow curves — alloys containing 2 wt% Fe, sharp yield point is observed.

Complete flow curves were recorded for each measured sample. Flow curves for each alloy are depicted in Figs. 3–5. Figure 3 shows flow curves of alloys containing Si. These flow curves are rather typical for $\beta$-titanium alloys in a solution treated condition [19]. Plastic deformation is accompanied only by a low work hardening.

Figure 4 shows flow curves of alloys containing 2 wt% of Fe. The yield point is followed by short work softening and subsequent work hardening. The yield point resembles the sharp yield point that is commonly observed in some steels when dislocations are released from the surrounding atmosphere of carbon atoms [20]. Such a sharp yield point was also observed in titanium and related bcc alloys and was attributed to either rapid dislocation multiplication, omega particles cut by gliding dislocations or even hydrogen content [21–23]. In this case,

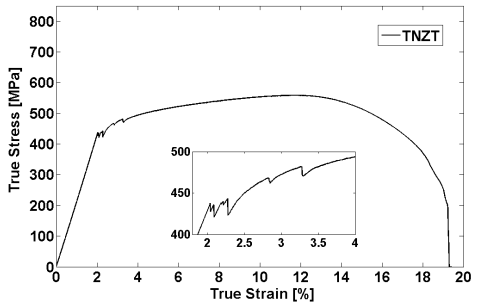


Fig. 5. Flow curve — initial TNZT alloy, insert shows details of the serrated yield behaviour.

the sharp yield point is probably caused by solute atoms of Fe. These atoms cause distortion of crystallographic lattice attracting (or pinning) dislocations during forging. During tensile test these dislocations are pulled out from these preferential sites causing short work softening. Short softening is followed by pronounced work hardening during more than 15% of straining for TNZT–2Fe alloy followed by a long evolution of necking and failure. For TNZT–2Fe–0.5Si, the uniform elongation is shorter and also the neck is less ductile. It follows that 2 wt% of Fe create sufficient obstacles for dislocation motion causing dislocation multiplication responsible for work hardening. 1 wt% of Fe is insufficient in this respect. Thanks to work hardening, the specimen undergoes longer uniform elongation before the limit of stability of plastic flow is reached [24]. Therefore the alloy with 2 wt% Fe shows both increased strength and ductility.

Figure 5 shows the true-stress true-strain flow curve for the benchmark TNZT alloy that is intentionally showed as the last one. The reason is the unusual behaviour around the yield point, which is highlighted in the inset. Note that those distinctive stress jumps in the flow curve were accompanied by a clearly audible acoustic emission (i.e. the acoustic emission was just audible with no equipment) Proper acoustic emission measurement was therefore used during the next set of tensile tests.

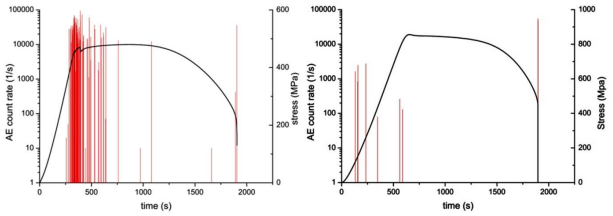


Fig. 6. (a) Acoustic emission (AE) during tensile test of benchmark TNZT alloy. Flow curve is represented by solid black line and AE is shown in red. High intensity of AE is observed around yield point. (b) representative example of low acoustic emission observed for all other alloys. Flow curve is represented by a solid black line and AE is shown in red.

Figure 6a shows the flow curve for the benchmark TNZT alloy along with the acoustic emission signal. Not surprisingly, the high intensity of the acoustic emission was measured around the yield point and is obviously associated with the serrated yielding. Acoustic emission was measured also for samples from other alloys. The AE signal for these alloys was incomparably lower and not concentrated around a yield point. An example of such behaviour is given in Fig. 6b.

Even a detailed inspection of the flow curve in Fig. 5 did not reveal any jumps/serrations in the rest of the flow curve after the yield point. Several explanations of such serrated yielding of beta titanium alloys were proposed. The first one is the twinning in Ti alloys with bcc structure [25–28]. Another explanation is the interaction between dislocations and solute/interstitial atoms. However, such mechanism requires sufficient mobility of solute/interstitial atoms during the test. Finally, a completely different mechanism was proposed by Banerjee and Naik [29]. The authors assumed that load drops are caused by deformation bands within which omega particles are destroyed and dislocations can freely move.

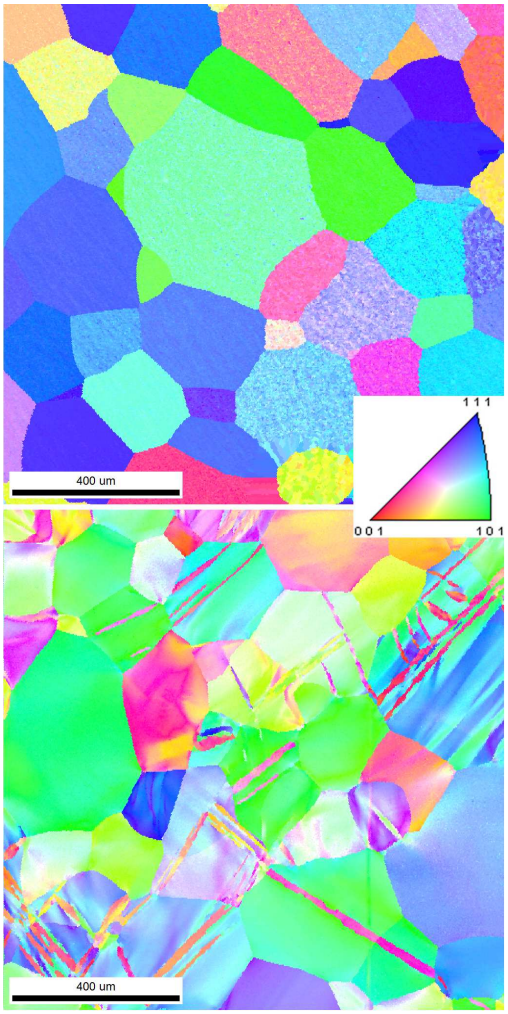


Fig. 7. (a) TNTZ, nondeformed part. (b) TNTZ, active part. In the insets there is color coding — orientation triangle for the bcc structure.

EBSD analysis was undertaken in order to identify the deformation mechanism causing the serrated yielding. EBSD images of respectively the nondeformed and the active part of the same sample after fracture are shown in Fig. 7a and b. The nondeformed part shows coarse grained recrystallized structure. The image is a little blurred, because of poor surface quality of the specimen and the consequent extensive software clearing of the raw EBSD image. Figure 7b shows the twinned structure and deformed coarse grains. The concentration of twins is comparatively low [27]. Twin nucleation is associated with serrated yielding; however, it remains unclear why the concentration of twins remain quite low and why the serrated yielding occurs only around the yield point.

## 4. Conclusions

Six different alloys based on the Ti–Nb–Zr–Ta alloy with various Fe and Si content were manufactured and their tensile properties were determined. The following conclusions can be drawn from this investigation:

1. The yield stress can be increased from 450 MPa to 700 MPa by small Fe and Si additions.
2. The Ti–35Nb–7Zr–5Ta alloy shows an unusual tensile behaviour with a serrated flow curve around the yield point. This can be attributed to twinning.
3. A small Fe content increases the plastic elongation thanks to work-hardening. The concentration of Fe (2 wt%) is sufficient for dislocation mutliplication during straining and also a sharp yield point is observed.
4. The alloy with composition Ti–35Nb–7Zr–5Ta–2Fe–0.5Si showed a maximum strength that is sufficient for biomedical use.

## Acknowledgments

The financial support by the Czech Science foundation under grant P107/12/1025 and the partial support by Grant Agency of Charles University under GAUK 158213 are gratefully acknowledged.

## References

[1] M. Geetha, A.K. Singh, R. Asokamani, A.K. Gogia, *Prog. Mater. Sci.* **54**, 397 (2009).

[2] H.J. Rack, J.I. Qazi, *Mater. Sci. Eng. C* **26**, 1269 (2006).

[3] M. Long, H.J. Rack, *Biomaterials* **19**, 1621 (1998).

[4] K.S. Katti, *Coll. Surf. B Biointerfaces* 39, 133 (2004).

[5] Y. Okazaki, E. Gotoh, *Biomaterials* **26**, 11 (2005).

[6] S. Rao, Y. Okazaki, T. Tateishi, T. Ushida, Y. Ito, *Mater. Sci. Eng. C* **4**, 311 (1997).

[7] M. Abdel-Hady Gepreel, M. Niinomi, *J. Mech. Behav. Biomed. Mater.* **20**, 407 (2013).

[8] D. Kuroda, M. Niinomi, M. Morinaga, Y. Kato, T. Yashiro, *Mater. Sci. Eng. A* **243**, 244 (1998).

[9] T. Ahmed, H.J. Rack, Alloy of titanium, zirconium, niobium and tantalum for prosthetics, US Patent 5871595 A, 1999.

[10] P.L. Ferrandini, F.F. Cardoso, S.A. Souza, C.R. Afonso, R. Caram, *J. Alloys Comp.* **433**, 207 (2007).

[11] N. Sakaguchi, M. Niinomi, T. Akahori, J. Takeda, H. Toda, *Mater. Sci. Eng. C* **25**, 370 (2005).

[12] E.W. Collings, H.L. Gegel, *Scr. Metall.* **7**, 437 (1973).

[13] S. Ankem, D. Banerjee, D.J. McNeish, J.C. Williams, S.R. Seagle, *Metall. Trans. A* **18**, 2015 (1987).

[14] T.J. Headley, H.J. Rack, *Metall. Trans. A* **10**, 909 (1979).

[15] G. Welsch, R. Boyer, E.W. Collings, *Materials Properties Handbook: Titanium Alloys*, ASM International, Materials Park, Ohio, USA 1993.

[16] K. Chaudhuri, J.H. Perepezko, *Metall. Trans. A* **25**, 1109 (1994).

[17] J. Bohlen, F. Chmelík, P. Dobroň, D. Letzig, P. Lukáč, K.U. Kainer, *J. Alloys Comp.* **378**, 214 (2004).

[18] P. Dobroň, F. Chmelík, K. Parfenenko, D. Letzig, J. Bohlen, *Acta Phys. Pol. A* **122**, 593 (2012).

[19] K. Narita, M. Niinomi, M. Nakai, J. Hieda, K. Oribe, *J. Mech. Behav. Biomed. Mater.* **9**, 214 (2012).

[20] F.C. Campbell, *Elements of Metallurgy and Engineering Alloys*, ASM International, Materials Park, Ohio, USA 2008.

[21] I.S. Golovin, M.U. Kollerov, E.V. Schinaeva, *J. Phys. IV* **06**, 289 (1996).

[22] R.J. Grylls, S. Banerjee, S. Perungulam, R. Wheeler, H.L. Fraser, *Intermetallics* **6**, 749 (1998).

[23] X. Wang, H. Hamasaki, M. Yamamura, R. Yamauchi, T. Maeda, Y. Shirai, F. Yoshida, *Mater. Trans.* **50**, 1576 (2009).

[24] F. Geng, M. Niinomi, M. Nakai, *Mater. Sci. Eng. A* **528**, 5442 (2011).

[25] E. Bertrand, P. Castany, I. Péron, T. Gloriant, *Scr. Mater.* **64**, 1110 (2011).

[26] J.W. Christian, S. Mahajan, *Progr. Mater. Sci.* **39**, 1 (1995).

[27] X.H. Min, X. Chen, S. Emura, K. Tsuchiya, *Scr. Mater.* **69**, 393 (2013).

[28] X.H. Min, K. Tsuzaki, S. Emura, T. Sawaguchi, S. Ii, K. Tsuchiya, *Mater. Sci. Eng. A* **579**, 164 (2013).

[29] S. Banerjee, U.M. Naik, *Acta Mater.* **44**, 3667 (1996).